Numerical determination of vertical water flux based on soil temperature profiles

Alain Tabbagh, Bruno Cheviron, Hocine Henine, Roger Guérin, Mohamed-Amine Bechkit

Numerical determination of vertical water flux based on soil temperature profiles

Alain Tabbagh[1], Bruno Cheviron[2]; Hocine Henine[3], Roger Guérin[1], Mohamed-Amine Bechkit[4]

[1] Sorbonne Universités, UPMC Univ Paris 06, UMR 7619, METIS, F-75005, Paris, France

2 Irstea, UMR G-EAU, Domaine de Lavalette, 361 rue Jean-François Breton, 34196 Montpellier cedex 5, France

[3] Irstea, Hydrosystèmes et Bioprocédés, 1 rue Pierre-Gilles de Gennes, CS 10030, 92761 Antony cedex, France

[4] Université des Sciences et de la Technologie Houari Boumediene, BP 32 El Alia, 16111 Bab Ezzouar, Alger, Algeria

Corresponding author: Alain Tabbagh, +33 1 44274824, alain.tabbagh@upmc.fr

Abstract

High sensitivity temperature sensors (0.001 K sensitivity Pt100 thermistors), positioned at intervals of a few centimetres along a vertical soil profile, allow temperature measurements to be made which are sensitive to water flux through the soil. The development of high data storage capabilities now makes it possible to carry out *in situ* temperature recordings over long periods of time. By directly applying numerical models of convective and conductive heat transfer to experimental data recorded as a function of depth and time, it is possible to calculate Darcy's velocity from the convection transfer term, thus allowing water infiltration/exfiltration through the soil to be determined as a function of time between fixed depths.

In the present study we consider temperature data recorded at the Boissy-le-Châtel (Seine et Marne, France) experimental station between April 16th, 2009 and March 8th, 2010, at six different depths and 10-min time intervals. We make use of two numerical finite element models to solve the conduction/convection heat transfer equation and compare their merits. These two models allow us to calculate the corresponding convective flux rate every

day using a group of three sensors. The comparison of the two series of calculated values centred at 24 cm shows reliable results for periods longer than 8 days.

These results are transformed in infiltration/exfiltration value after determining the soil volumetric heat capacity. The comparison with the rainfall and evaporation data for periods of ten days shows a close accordance with the behaviour of the system governed by rainfall evaporation rate during winter and spring.

Keywords: Infiltration, unsaturated soil, numerical finite element models, Pt100 thermistor, temperature

1. Introduction

Since convection is a component of the heat transport process, water seepage can be in turn determined through the analysis of temperature measurements [1], [2], [3]. The analysis of the temperature distribution thus offers the possibility to determine the Darcy's velocity without knowing head gradients. Although this is an old idea, it is likely that it will be more extensively developed in the future as a result of the possibilities offered by a large panel of new technologies, which facilitate the acquisition and recording of data. As an example, temperature monitoring with a fibre optic sensor (distributed temperature sensing, DTS) [4], [5], [6], and [7] allows data to be recorded at high temporal and spatial densities and over long distances. High resolution sensors coupled with low power electronics and vast data storage capacities have also contributed to the development of renewed in-field applications involving temperature measurements, surveys and chronicles.

For more than fifty years, soil temperature monitoring has been applied to both saturated and unsaturated underground media. However researchers face a major difficulty: seepage velocities are generally low in temperate climate soil contexts (dominance of clay

loam, medium water contents, low rainfall intensities) thus the conductive heat transfer largely dominates that due to convection, which makes the Peclet number clearly smaller than 1. Measurements and calculations must therefore be very accurate, and a detailed description of the soil's conductive transfer is required to ensure that the convective component can be correctly evaluated.

The present paper deals with natural heat exchanges which allow the long-term analysis of water seepage. Our approach extends those exposed in a series of prior studies, which can be summarized as follows.

By considering a saturated medium (rice paddies) and high percolation rates, Suzuki [8] was the first to derive a method allowing percolation to be estimated from the amplitude ratio of sinusoidal temperature fluctuations along vertical profiles. Stallman [9] proposed an analytical solution, based on the attenuation of sinusoidal temperature fluctuations, which was applied to the case of an unsaturated medium and diurnal temperature fluctuations, leading to an ultimate accuracy of 1 mm d^{-1}. For deeper borehole measurements, where steady state conditions can be assumed, Bredehoeft and Papadopoulos [10] proposed an analytical solution taking both the conductive and convective transfers into account, which leads to an exponential variation of temperature as a function of depth, governed by Darcy's velocity. By making the same assumptions, several authors [11], [12], [13] compared, with satisfactory results, water flows obtained using this approach with those determined from hydrological data. Taniguchi [14] contributed several improvements to the unsteady state analytical approach, taking the amplitude and phase of sinusoidal time variations into account and distinguishing between infiltration and exfiltration. Contrary to Stallman [9], Taniguchi [14] based these calculations on annual temperature fluctuations. Complete analytical solutions to the conductive and convective transfer problem for sinusoidal and transient variations were proposed by Tabbagh *et al*. [15]. Other studies specifically analysed flow through streambeds

[16], [17], [18] and attempts have been made to develop a numerical approach for recharge determinations using borehole measurements [19]. Today a significant research effort is still involved in semi-analytical based Fourier models [3], [20]. All of these studies were based on the assumption of a homogeneous medium. Interpretation of layered terrain using analytical solutions is more complex. The study must be split into two steps: firstly determine the thermal structure, and then the Darcy velocity [21]. Such an algorithm has been applied to the determination of recharge rate, in the Seine river basin (France) over a period of several years [22] where a sufficiently dense network of meteorological stations exists. However, the calculation process remains complex. The main limitation of this process is the lack of resolution of the sensors (0.1 K in meteorological stations) which must be compensated for by stacking long series of data. However, stacking the data limits the recharge determination to multi-annual cycles, except in the case of significant transient thermal events accompanied by a sufficiently strong thermal signal [23].

In this study, we present a new framework and the first test of direct resolution models that rely on high precision sensors. The sensors are positioned at different depths of several centimetres along a vertical soil profile (see Figure 1) and temperature measurements are collected at short intervals over a period of several months. The infiltration/exfiltration is calculated through the use of simple numerical scheme(s) based on the finite element (FE) method, such that variations in the soil's thermal properties can be determined over a short distance or any desired time interval.

2. Materials and methods

2.1 Instrumentation

We make use of new Pt100 thermistors (Correge, France, http://www.correge.fr/) with a resolution of 0.001 K, together with a dedicated autonomous acquisition system allowing

102 measurement intervals of a few minutes to be achieved with the same 0.001 K resolution. The
103 sensors and the associate electronics were previously co-calibrated in laboratory in order to
104 correct for the slight offsets that exist between them [24].

105 The study plot of 614 m² surface is located at the experimental site of Boissy-le-Châtel
106 in the Orgeval catchment (70 km East of Paris, France) [25]
107 (http://data.datacite.org/10.17180/OBS.ORACLE). The annual average air temperature is
108 12°C. The area of this catchment is covered by a quaternary loess deposit whose maximum
109 thickness is 10 m. The top layer has evolved into hydromorphic gleyic luvisol (FAO soil
110 classification) that presents hydromorphic characteristics and may cause the formation of a
111 temporary perched water table in the winter season. The plot is artificially drained by buried
112 perforated pipes (buried at 0.6 m and separated by about 6 m) and managed for experimental
113 purposes, but unfortunately no measurement of the drained quantities was possible in 2009
114 and 2010. This plot is instrumented for a continuous monitoring (hourly recording) of
115 meteorological variables (air and soil temperature, net radiation, air pressure and relative
116 humidity). Based on the daily average of these variables, "Météo France" calculates potential
117 evapotranspiration by using the Penman formula [26]. This formula is consistent with the
118 canopy of the study site (grass). Rainfall was measured using tipping bucket rain gauge
119 (manufactured by "Précis mécanique", SA) and recorded each hour (the recording device is
120 Danae LC/RTC, from "Alcyr SARL").

121 For the initial experiment, the temperature sensors were installed at six different depths:
122 12, 15, 18, 24, 32 and 34 cm below ground surface, along the wall of an excavated pit (which
123 was later backfilled). The sensors were inserted into horizontally drilled guide-holes
124 (Figure 1), allowing them to be positioned at accurately known depths with inter-sensor
125 intervals ranging between 3 and 12 cm. The thermal diffusivity of the soil is characterised by
126 annual variations, ranging between 0.61 $x10^{-6}$ m^2 s^{-1} during dry periods and 0.43 $x10^{-6}$ m^2 s^{-1}

during wet periods and can be used to monitor the soil water content [4], [27]. The temperature recorder and electronic equipment were installed in metal boxes placed on the land surface in the lawn. Sensor configuration and data acquisition were achieved via a serial port on a portable micro-computer, using interfaces produced in our laboratory. Continuous recording began on April 16th, 2009 and ended on March 8th, 2010, corresponding to a total of 327 days, and was interrupted 4 times, on June 30th, September 21st, December 16th, 2009 and February 10th, 2010 in order to change the battery. The 12 cm sensor did not function between May 22nd and June 30th, 2009. Data were recorded at 10-min intervals, leading to a total of 144 discrete measurements per 24-hour period. As the calculations are based upon the time evolution of temperature differences between close sensors, a high resolution is required for the temperature monitoring system; this is illustrated in Figure 2, which plots the variations of the temperature recorded on April 16th and 17th, 2009, and of the difference between two sensors. The temperature variation shows both an amplitude decrease and a phase lag increase with depth. For each curve are drawn the data directly recorded with a 0.001K resolution and the data which we would have with a 0.1K resolution. Figures 2b and 2c show the difference of temperature between couples of sensors, they demonstrate the significant differences between the 0.1 K and 0.001 K resolutions.

2.2 Calculations

We assume that the heat generated/absorbed by vaporization, condensation, chemical or biologic activity can be neglected in the considered range of depth, so as the mass and thermal fluxes associated with vapour diffusion. Consequently in absence of local heat source or sink the unsteady conductive heat transfer is governed by the thermal diffusivity, Γ, and the unsteady convective heat transfer by the flux rate, v, and the temperature distribution is thus

controlled by these two parameters only. When only considering the vertical dimension, z (1D geometrical problem), the heat equation is expressed as:

$$\frac{\partial}{\partial z}\left(\Gamma\frac{\partial T}{\partial z}\right)-\frac{\partial}{\partial z}(vT)-\frac{\partial T}{\partial t}=0 \qquad (1).$$

The diffusivity (m^2s^{-1}) of the three-phase soil integrates both the thermal conductivity, λ ($W\ m^{-1}\ K^{-1}$) and the volumetric heat capacity, C_v in ($J\ m^{-3}\ K^{-1}$), whereas the flow rate ($m\ s^{-1}$) integrates the Darcy's velocity, u, and the ratio of the volumetric capacity of the fluid, C_w, to that of the three-phase medium:

$$\Gamma(z,t)=\frac{\lambda(z,t)}{C_v(z,t)} \qquad (2)$$

$$v(z,t)=\frac{u(z,t)C_w}{C_v(z,t)} \qquad (3).$$

When using the FE method equation (1) is integrated over definite size elements. To achieve this integration the variations of all parameters must be chosen. By applying the Galerkin method to triangular two-dimensional (2D) elements defined in the dimensions of depth and time, it is possible to start from this second order differential equation and to integrate by parts using linear variations on the elements.

As illustrated by Figure 1, only three different depths are needed, corresponding to the spatial limits defined by the elements [i-1, i] and [i, i+1] of respective steps h_i and h_{i+1}. The time variable lies within the two steps: [m-1, m] and [m, m+1] of constant size τ. Γ and v are defined at three consecutive spatial nodes and assumed to vary linearly in z over each element. Because, following equation (1), only the temperature exhibits time derivation, there is no possibility at a given time step to consider a variation of Γ and v with time, they are thus constant but they vary with considered time intervals. Thus one uses six spatial unknowns Γ_{i-1}, Γ_i, Γ_{i+1}, v_{i-1}, v_i and v_{i+1}. Depending on the number of nodes considered in the spatial and time discretization, two models are proposed (Figure 1): the first model involves nine nodes

and the second use five nodes by omitting the corner nodes. The discretization of equation (1) with the nine-node model yields:

$$
\begin{aligned}
&\frac{\tau}{2h_{i+1}}(\Gamma_i+\Gamma_{i+1})\left[\frac{2}{3}(T_{i+1}^{m}-T_i^{m})+\frac{1}{6}(T_{i+1}^{m+1}-T_i^{m+1}+T_{i+1}^{m-1}-T_i^{m-1})\right]\\
&-\frac{\tau}{2h_i}(\Gamma_i+\Gamma_{i-1})\left[\frac{2}{3}(T_i^{m}-T_{i-1}^{m})+\frac{1}{6}(T_i^{m+1}-T_{i-1}^{m+1}+T_i^{m-1}-T_{i-1}^{m-1})\right]\\
&-\frac{\nu_i\tau}{9}\left[4T_i^{m}+T_{i-1}^{m}+T_{i+1}^{m}+T_i^{m-1}+T_i^{m+1}+\frac{1}{4}(T_{i-1}^{m-1}+T_{i-1}^{m+1}+T_{i+1}^{m-1}+T_{i+1}^{m+1})\right]\\
&-\frac{\nu_{i-1}\tau}{9}\left[2T_{i-1}^{m}+T_i^{m}+\frac{1}{2}(T_{i-1}^{m-1}+T_{i-1}^{m+1})+\frac{1}{4}(T_i^{m-1}+T_i^{m+1})\right]\\
&-\frac{\nu_{i+1}\tau}{9}\left[2T_{i+1}^{m}+T_i^{m}+\frac{1}{2}(T_{i+1}^{m-1}+T_{i+1}^{m+1})+\frac{1}{4}(T_i^{m-1}+T_i^{m+1})\right]\\
&=\frac{1}{2}\left[(T_i^{m+1}-T_i^{m-1})(\frac{h_{i+1}+h_i}{3})+(T_{i-1}^{m+1}-T_{i-1}^{m-1})\frac{h_i}{6}+(T_{i+1}^{m+1}-T_{i+1}^{m-1})\frac{h_{i+1}}{6}\right]
\end{aligned}
\qquad (4)
$$

The discretization of equation (1) with the five-node model yields a shorter expression:

$$
\begin{aligned}
&-\frac{\tau}{2h_i}(\Gamma_i+\Gamma_{i-1})(T_i^{m}-T_{i-1}^{m})+\frac{\tau}{2h_{i+1}}(\Gamma_i+\Gamma_{i+1})(T_{i+1}^{m}-T_i^{m})\\
&-\frac{\nu_i\tau}{6}(4T_i^{m}+T_{i-1}^{m}+T_{i+1}^{m})-\frac{\nu_{i-1}\tau}{6}(2T_{i-1}^{m}+T_i^{m})-\frac{\nu_{i+1}\tau}{6}(2T_{i+1}^{m}+T_i^{m})\\
&=\frac{h_{i+1}+h_i}{4}(T_i^{m+1}-T_i^{m-1})
\end{aligned}
\qquad (5)
$$

The linear expressions (4) and (5) allow the diffusivity and convection terms to be calculated directly from known values of temperature, depth of the sensors and sampling time steps. Moreover, the use of a 10-min time step makes it possible to verify the stability condition:

$$\frac{\Gamma\tau}{h^2}\le\frac{1}{2} \qquad (6)$$

over a wide range of diffusivities (this corresponds to $\Gamma<0.75 \times 10^{-6}$ m^2 s^{-1} for h=3 cm and $\Gamma<3 \times 10^{-6}$ m^2 s^{-1} for h=6 cm) allowing most situations encountered in the field to be covered.

These two independent models of equations (4) and (5) were implemented in parallel to determine the values of Γ and v, so as to perform crosschecking and evaluate their

187 robustness. Following a series of tests both on synthetic data generated by analytical
188 calculation (using realistic soil properties and temperature variations) and Boissy-le-Châtel
189 data, the more stable solution was to consider successive temperatures at levels i-1 and i+1 as
190 Dirichlet limiting conditions, then to search for the values of Γ_{i-1}, Γ_i , Γ_{i+1}, v_{i-1}, v_i and v_{i+1}
191 allowing the best (least squares) fit between the calculated and recorded values of $T_{i,m}$ over a
192 sufficiently long calculation interval. The later was taken as the diurnal cycle (i.e. 144 time
193 steps of 10 min) or a multiple of it. The computational workflow can thus be broken down
194 into two steps:

195 - definition of the *a priori* values: u=0 and $\Gamma_{i-1}=\Gamma_i=\Gamma_{i+1}$, the latter of which being equal
196 to the optimal least squares value computed using finite differences applied to the
197 simple conduction equation,

198 - application of a damped least squares process [28] to calculate the six unknowns in
199 equations (4) or (5) where the convergence of the process is controlled by the
200 minimum of the criterion S defined by:

201 $$S = \sqrt{\left(\frac{\delta\Gamma_{i-1}}{\Gamma_{i-1}}\right)^2 + \left(\frac{\delta\Gamma_i}{\Gamma_i}\right)^2 + \left(\frac{\delta\Gamma_{i+1}}{\Gamma_{i+1}}\right)^2} + \mu\left|\delta v_{i-1} + 2\delta v_i + \delta v_{i+1}\right| \qquad (7),$$

202 with $\mu=10^7$ if v is expressed in m s^{-1}.

203 This process allows taking into account the significant difference in magnitude between the
204 conductive and convective heat fluxes. As an example, for a 1.5 W m^{-1} K^{-1} conductivity and a
205 temperature difference of 1K over 10 cm (see Figure 1) the order of magnitude of the
206 conductive heat flux is 15 W m^{-2}. For a 4 mm d^{-1} Darcy velocity and a fluid temperature
207 differing of 1K from the reference temperature, the order of magnitude of the convective heat

208 flux is 0.14 W m^{-2}. However the limited range of variation of the thermal diffusivity stabilizes
209 the numerical results.

210

211 **3. Results of the calculation and discussion**

212 The choice of high precision sensors prevents uncertainties resulting from temperature
213 measurements but the choice of simple numeric schemes to describe the time and depth
214 variations of the temperature may be too crude to deliver accurate values of Γ and v. To assess
215 this issue we compare at a given central depth, z=24 cm, the two numerical schemes
216 (equations (4) and (5)) with a triad of sensors located at 15, 24 and 34 cm. Figure 3 plots the
217 results of the calculations of v_i centred at 24 cm showing the calculated daily values (thin line)
218 and 10 days values (thick line) using five node-equation (4) (in blue) and nine node-equation
219 (5) (in red). Globally the 10 days values exhibit very coherent results in accordance with the
220 general vegetation behaviour: the calculated flow is upward during spring and the beginning
221 of summer, followed by a downward flow during autumn and winter. On the other hand daily
222 values exhibit a significant level of noise which forbids their direct use. The same difference
223 between daily and 10-day calculations arises for the determination of diffusivity (Figure 4).
224 The differences between the two numerical schemes stay very small here, except at one point
225 at the end of June where data are missing.

226 The role of the considered time interval in the calculations results from two facts: (1)
227 the geometric scale of the temperature sensor locations, (2) the linear depth and time
228 variations adopted in the F.E. schemes. The choice of the geometric scale derives from both
229 the respect of the 'Elementary Representative Volume' (at least centimetric) and of the
230 diameter of the sensor encapsulation (5.7 mm). In the context of this study, because of small
231 Darcy velocities, the transit time between two sensors necessitates several days (with a 3
232 $mm.d^{-1}$ velocity a 3 cm distance is travelled in 10 days). The differences that may result from

233 the imperfect fit between linear schemes and the actual time and depth variations is illustrated
234 by the discrepancies between the results obtained by the 5-node and the 9-node schemes.
235 However, these discrepancies remain lower than 1 mm d^{-1} in the 10 days calculations
236 presented here and the 9-node scheme predicts slightly greater amplitudes.

237 To assess the robustness of calculations one first considers the mean quadratic
238 deviations when the vertical location of one of the sensors is moved by 1 mm for a one
239 diurnal cycle interval calculation (Table 1). As could be expected, the deviations are maximal
240 when the central sensor is moved (introducing variations in two pairs of depths instead of
241 one) but they remain limited to a far less than 1 mm d^{-1}.

242 The elementary statistics for the two one diurnal cycle calculations are presented in
243 Table 2. They show an absence of bias, all the means and medians remaining in a 0.4 mm d^{-1}
244 interval, and a greater variability in the nine-point scheme results than in the five-point one.
245 The coherences (the correlation coefficient between two spectra) between the curves are very
246 high (Table 3) but the partition of each spectrum in four quarters (for a 1 day time step, the
247 spectrum extends from 0 to 0.5 d^{-1} frequency and this interval is divided in four parts) shows
248 that the coherence originates in the first quarter, that is for frequencies lower than 0.125 d^{-1}
249 (periods of 8 days). The coherences obtained when comparing the flow rates calculated with
250 equation (5) for two different groups of sensors [15, 24 and 34 cm] and [18, 24 and 32 cm]
251 (Table 4) also exhibits a very high value for the first quarter. These strong coherences
252 therefore demonstrate that the water movement is reliably determined for slow temporal
253 variations.

254

255 **4. Determination of the Darcy velocity**

256 For the following steps of the infiltration/exfiltration calculation we will thus use the
257 'best' of the available results: those having the lowest variance, i.e. the lowest interquartile

distance for both v_i and Γ_i which correspond to the case for which the distances between the sensors are the most regular (sensors at 15, 24 and 34 cm), and also to the simplest, five nodes numerical expression.

The volumetric heat capacity C_v is needed in order to determine the infiltration or exfiltration (the Darcy velocity) using: $u = \frac{\nu C_v}{C_w}$. This C_v value may be determined from the combination of two relationships. The first, empirical, was proposed for the heat capacity by de Vries [29]:

$$C_v = (1-n)C_s + \theta C_w \qquad (8),$$

where C_s is the volumetric heat capacity of the solid fraction, n the porosity and θ the volumetric water content. The second relationship, obtained by combining empirical data and numerical modelling, was proposed for the thermal conductivity by Cosenza *et al*. [30]:

$$\lambda=(0.8908-1.0959n)\lambda_s+(1.2236-0.3485n)\theta \qquad (9),$$

where λ_s is the thermal conductivity of the solid fraction (also noting that the two first numerical constant are dimensionless while the two others have the dimension of a thermal conductivity).

In these two relationships C_w is constant (C_w=4.185 MJ m^{-3} K^{-1}), C_s can be considered as constant (C_s=2.0 MJ m^{-3} K^{-1}), while λ_s and n are variable with z (and site dependent) but constant with t; only θ is time variable. Both (8) and (9) have a linear dependence on θ. Consequently, their combination allows eliminating θ which results in a direct correspondence between the volumetric heat capacity (C_v) and the thermal diffusivity (Γ):

$$C_v = \frac{\alpha}{\Gamma - \beta} \qquad (10),$$

$$\text{where } \alpha = (0.8908-1.0959n)\lambda_s - \frac{C_s}{C_w}(1-n)(1.2236-0.3485n) \qquad (11),$$

and $\beta = \frac{(1.2236 - 0.3485n)}{C_w}$ (12).

For the case of the Boissy-le-Châtel site at 24 cm depth one has n=0.48 and λ_s=2.15 W m^{-1} K^{-1}, α=0.5218 W m^{-1} K^{-1} and β=0.2523 x 10^{-6} m^2 s^{-1}.

The simulated Darcy velocities, calculated over ten-day periods, were compared with the surface rainfall and Penman potential evapotranspiration (PET) at Boissy-le-Châtel (Figure 5). In an overview, this figure shows negative infiltration rates during spring and the beginning of summer (from April 16th to middle July) then positive infiltration rates with higher values during winter (from December 16th, 2009 to March 8th, 2010). In the first period upwards water movements dominate, they likely result from capillarity and hydraulic gradients created by root water uptake in the first 10 cm above. The calculated negative infiltration decreases and crosses zero value in July. In July and August, the model results show a positive infiltration while no rainfall occurs and potential evapotranspiration is high, but with a probable low real evapotranspiration (mainly due to the evaporation part as the roots were mostly inactive). In October and the beginning of November the infiltration is small at 24 cm while the rain is high and the potential evapotranspiration small. In accordance with these two observations, the correlation function between rain at soil surface and infiltration at 24 cm shows a maximum for a 75 day delay on the total period of 327 days. In winter period nearly saturated soils favour downwards water movements that follow gravity. During summer this high delay is much likely even higher because the low water contents of the most superficial layers tend to hamper water displacements.

For the whole period, the calculated infiltration is negatively correlated with PET (the Pearson coefficient is -0.61 for the 327 day period). The global recharge measured over this period was 158 mm.

5 More about the applicability and requirements of the method

Whereas the present paper establishes the feasibility of the direct calculation of water movements from triads of high-resolution temperature sensors, it seems daring to draw general conclusions about the robustness, applicability and limits of the method: other experiments in similar and different soil contexts are certainly necessary. These will start after delineating the requirements about the measurement parameters themselves, first with indications on the spatial and temporal patterns of data acquisition, then with the most crucial argument on the resolution of the temperature measurements.

- The choice of the vertical spacing (section 3 above) is limited by the soil inhomogeneity (REV) and by the size of the sensor encapsulation.
- - The up-to-date recording facilities allow easy adjustment of the recording, thus of calculation time steps, so that the temporal aspect is not a limitation for the method.
- - The question of the temperature resolution is of greater importance: to which limit is it possible to reduce this resolution keeping in mind that DTS cannot offer more than 0.03K? This point can be dealt by considering worse resolutions: 0.01K and 0.1K.

Figures 6a and 7a present the time variations of the flow rates obtained for one day periods with the 0.001K resolution (red lines), 0.01K resolution (green lines) and 0.1K resolution (blue lines). It can be observed that while the general seasonal trend is preserved, the noise level becomes significant and is roughly equivalent for 0.01K and 0.1K. This is confirmed by looking at the variograms (Figures 6b and 7b): at 0.001K resolution, the variogram level remains smaller than at 0.01K or 0.1K with a reduced nugget effect, and a plateau beginning at 100 lag-days. It must be underlined that the variograms for the thermal diffusivities (Figures 6c and 7c) do not show similar features as the differences between the three variograms remaining small. This is explained by the dominance of the conduction transfer over the convection one, for which the 0.001K resolution is required in this experiment.

6 Conclusions

In the soil and climate conditions considered here, the heat transfer by conduction is usually about one order of magnitude larger than the convection transfer in the unsaturated soil, which makes difficult the determination of the Darcy velocity from temperature measurements. However, the direct calculation of this velocity is of high interest and possible with temperature sensors of sufficient resolution, for time periods greater than a week, with minimal assumptions about soil structure and characteristics. Moreover, the method neither requires the prior knowledge of the hydrodynamic parameters nor any assumption regarding the form of the temperature variations with time and depth.

In summary, we have presented here the first experiment where the limitations resulting from the use of conventional low-sensitivity (0.1 K) temperature sensors are overcome by using 0.001 K sensors. Rather than complex analytical calculations we adopted simple FE numerical schemes and a (least squares) stack over multiples of the 24h period. The recording of temperature measurements at centimetric spatial and several minutes temporal intervals, and the use of simple numerical models are straightforward and relatively uncomplicated when compared to other more common techniques, such as lysimeters, used for the *in situ* determination of infiltration and recharge. The implementation of the whole system (sensors, computational tools) stays rather cheap.

The daily values calculated with two different numerical schemes yet exhibits a significant dispersion but this dispersion corresponds to higher frequencies and the coherence of the lower frequency variations are very high; the ten-day periods results are reliable in accordance with local potential flux data. To go further and to reach a day to day determination of the infiltration would necessitate reducing the distance between the sensors due to the order of magnitude of the Darcy's velocity: a few millimetres per day. This

corresponds to a great challenge because too small geometric scales can be incompatible with the representation of the soil by a continuous medium. Conversely, contexts characterised by higher seepage velocities would be more favourable for the method.

The methodological development exposed here should be considered as a new tool in an expanding toolbox, which can allow new avenues to be explored in the study of critical zone water displacements, in both hydrological and agricultural fields of application. Future progresses would especially address 2D and 3D problems or the inclusion of additional terms in the heat equation to handle thermal fluxes in the vapour phase [31], a possible objective being the location of the evaporation front. High precision temperature measurements also merit to be tested for distinguishing between the different types of liquid water flows in soils, typically in the micro- and macro-porosity [32].

Acknowledgments

The present study would not have been possible without the support of the IRSTEA (French Research Institute for Science and Technology in the Environment and Agriculture, previously the Cemagref), which provided the authors with access to its BD_ORACLE database (http://data.datacite.org/10.17180/OBS.ORACLE) and relevant complementary data, as well as to the experimental site at Boissy-le-Châtel (Seine et Marne, France) part of the critical zone observatory ORACLE.

References

[1] Anderson M. P., Heat as a ground water tracer. Groundwater 2005; 43: 951-968.

[2] Constantz J., Heat as a tracer to determine streambed water exchanges. Water Resources Research 2008; 44: W00D10 doi:10.1029/2008WR00699.

[3] Rau G. C., Andersen M. S., McCallum A. M. Roshan H. and Acworth R. I., Heat as a tracer to quantify water flow in near-surface sediments. Earth-Science Review 2014; 129: 40-58.

[4] Steele-Dunne S., Rutten M., Krzeminska D., Hausner M., Tyler S. W., Selker J.,Bogaard T. and van De Giesen N., Feasibility of soil moisture estimation using passive distributed temperature sensing. Water Resources Research 2010, 46-3, W03534.

[5] Slater L. D., Ntarlagiannis D., Day-Lewis F. D., Mwakanyamale K., Versteeg R. J., Ward A., Strickland C., Johnson C. D. and Lane Jr. J. W., Use of electrical imaging and distributed temperature sensing methods to characterize surface water groundwater exchange regulating uranium transport at the Hanford 300 Area, Washington. Water Resources Research 2010; 46: W10533 doi:10:1029/2010WR009110.

[6] Briggs M. A., Lautz L. K., McKenzie J. M., Gordon R. P. and Hare D. K., Using high-resolution distributed temperature sensing to quantify spatial and temporal variability in vertical hyporheic flux. Water Resources Research 2012; 48: W02527.

[7] Read T., Bour O., Bense V., Le Borgne T., Goderniaux P., Klepikova M.V., Hochreutener R., Lavenant N. and Boschero V., Characterizing groundwater flow and heat transport in fractured rock using fiber-optic distributed temperature sensing. Geophysical Research Letters 2013; 40: 2055-2059.

[8] Suzuki S., Percolation measurements based on heat flow through soil with special reference to paddy fields. Journal of Geophysical Research 1960; 65: 2883-2885.

399 [9] Stallman R. W., Steady one-dimensional fluid flow in a semi-infinite porous medium with
400 sinusoidal surface temperature. Journal of Geophysical Research 1965; 70: 2821-2827.
401 [10] Bredehoeft J. D. and Papadopoulos I., Rates of vertical groundwater movement estimated
402 form the Earth's thermal profiles. Water Resources Research 1965; 1: 325-328.
403 [11] Stallman R. W., Flow in the zone of aeration. Advances in Hydroscience. Academic
404 Press, New York, 1967; 4: 151-195.
405 [12] Sorey M. L., Measurement of vertical groundwater velocity from temperature profiles in
406 wells. Water Resources Research 1971; 7: 963-970.
407 [13] Boyle J. M. and Saleem Z. A., Determination of recharge rates using temperature-depth
408 profiles in wells. Water Resources Research 1979; 15: 1616-1622.
409 [14] Taniguchi M., Evaluation of vertical groundwater fluxes and thermal properties of
410 aquifers based on transient temperature–depth profiles. Water Resources Research 1993; 29:
411 2021-2026.
412 [15] Tabbagh A., Bendjoudi H. and Benderitter Y., Determination of recharge in unsaturated
413 soils using temperature monitoring. Water Resources Research 1999; 35: 2439-2446.
414 [16] Constantz J., Stewart A. E., Niswonger R., and Sarma L., Analysis of temperature profile
415 for investigating stream losses beneath ephemeral channels, Water Resources Research 2002;
416 38:1316 doi:10.1029/2001WR001221.
417 [17] Keery J., Binley A., Crook N. and Smith J. W. N., Temporal and spatial variability of
418 groundwater-surface water fluxes: Development and application of an analytical method
419 using temperature time series. Journal of Hydrology 2007; 336: 1-16.
420 [18] Roshan H., Rau G. C., Andersen M. S. and Acworth I. R., Use of heat as tracer to
421 quantify vertical streambed flow in a two-dimensional flow field. Water Resources Research
422 2012; 48: W10508 doi:10.1029/2012WR011918.

423 [19] Keshari A. K. and Koo M.-H., A numerical model for estimating groundwater flux from
424 subsurface temperature profiles. Hydrological Processes 2007; 21: 3440-3448.
425 [20] Halloran L. J. S., Roshan H., Rau G. C., Andersen M. S., Calculating water saturation
426 from passive temperature measurements in near-surface sediments: Development of a semi-
427 analytical model, Advances in Water resources2016; 89: 67-79.
428 [21] Cheviron B., Guérin R., Tabbagh A. and Bendjoudi H., Determining long-term effective
429 groundwater recharge by analysing vertical soil temperature profiles at meteorological
430 stations. Water Resources Research 2005; 41: W09501, doi:10.1029/2005WR004174.
431 [22] Tabbagh A., Guérin R., Bendjoudi H., Cheviron B. and Bechkit M.-A., Pluri-annual
432 recharge assessment using vertical soil temperature profiles: Example of the Seine river basin
433 (1984–2001). Comptes Rendus Geoscience 2009; 341: 949–956.
434 [23] Bendjoudi H., Cheviron B., Guérin R. and Tabbagh A., Determination of
435 upward/downward groundwater fluxes using transient variations of soil profile temperature:
436 test of the method with Voyons (Aube, France) experimental data. Hydrological Processes
437 2005 ; 19 : 3735-3745.
438 [24] Bechkit M.-A., Sur la détermination de la teneur en eau et de l'infiltration à partir de
439 mesures passives de la température du sol. Thèse de doctorat, Université Pierre et Marie
440 Curie-Paris 6 2011 ; 162 p.
441 [25] Mouhri A., Flipo N., Rejiba F., de Fouquet C., Bodet L., Kurtulus B., Tallec G., Durand
442 V., Jost A., Ansart P. and Goblet P., Designing a multi-scale sampling system of stream-
443 aquifer interfaces in a sedimentary basin. Journal of Hydrology 2013; 504: 194-206.
444 [26] Penman H. L., Natural evaporation from open water, bare soil and grass. Proceedings of
445 the Royal Society London 1948; A193: 120-146.
446 [27] Bechkit M.-A., Flageul S., Guérin R. and Tabbagh A., Monitoring soil water content by
447 vertical temperature variations. Groundwater 2014; 52: 566-572.

448 [28] Marquardt D. W., An algorithm for least-square estimation of nonlinear parameters.
449 Journal of the Society for Industrial and Applied Mathematics 1963; 11: 431-441.
450 [29] de Vries D.A., Thermal properties of soils. In: Physics of Plant Environment, edited by
451 W.R. van Wijk, North-Holland Publishing Company, Amsterdam 1963; 210-235.
452 [30] Cosenza P., Guérin R. and Tabbagh A., Relationship between thermal conductivity and
453 water content of soils using numerical modelling. European Journal of Soil Science 2003; 54:
454 581-587.
455 [31] Saito H., Simunek J., Mohanty B. P. Numerical analysis of coupled water, vapour and
456 heat transport in the vadose zone. Vadose Zone Journal 2006; 5: 784-800.
457 [32] Vogel T., Dohnal M., Votrubova J., Modelling heat fluxes in macroporous soil under
458 sparse young forest of temperate humid climate. Journal of Hydrology 2011; 402: 367-376.
459

460 **Figure captions**

461 Figure 1: Sensor installation at Boissy-le-Châtel experimental station: location, horizontal
462 holes for the insertion in the wall of the excavated pit, FE depth and time scheme.

463

464 Figure 2: Plot of the temperatures (a) and of the differences (b) in temperature variations at
465 10 min intervals recorded with a 0.001 K sensitivity on April 16th and 17th, 2009 at the
466 Boissy-le-Châtel experimental station. For comparison to existing technology, the recorded
467 data we would have at each sensor for a 0.1 resolution is shown and the plot (c) details the
468 grey zone of plot (b).

469

470 Figure 3: Convective flux rate at 24 cm determined by the two different calculation schemes
471 (equation (4) in red and equation (5) in blue). The daily values correspond to thin lines and the
472 10 days values to thick lines.

473

474 Figure 4: Thermal diffusivity at 24 cm determined by the two different calculation schemes
475 (equation (4) in red and equation (5) in blue). The daily values correspond to thin lines and
476 the 10 days values to thick lines.

477

478 Figure 5: Comparison between infiltration values calculated for 10 days intervals, surface
479 rainfall and potential evapotranspiration (rain, in red, PET in blue).

480

481 Figure 6: (a) Time variations of the flow rates obtained for one day periods with the 0.001K
482 resolution (red line), 0.01K resolution (green line) and 0.1K resolution (blue line), (b)
483 variogram of the flow rate calculated with one day periods, (c) variogram of the thermal
484 diffusivity calculated with one day periods.

Figure 7: (a) Time variations of the flow rates obtained for ten days periods with the 0.001K resolution (red line), 0.01K resolution (green line) and 0.1K resolution (blue line), (b) variogram of the flow rate calculated with ten days periods, (c) variogram of the thermal diffusivity calculated with ten days periods.

491

492 **Table captions**

493 Table 1: Mean quadratic deviations, $e = \frac{1}{N}\sum_{1}^{N} \sqrt{(v_{0,i} - v_{1,i})^2}$, between the calculated flow

494 rate with exact sensor location, $v_{0,}$ and the flow rate when one sensor is moved of 1 mm, v_1.

495

496 Table 2: Means, standard deviations, medians and interquartile distances delivered by the two

497 different calculation schemes.

498

499 Table 3: Coherences for the different parts of the spectrum between the two different

500 calculation schemes.

501

502 Table 4: Coherences for the different parts of the spectrum between the two different triads of

503 sensors (15, 24 and 34 cm) and (18, 24 and 32 cm).

504

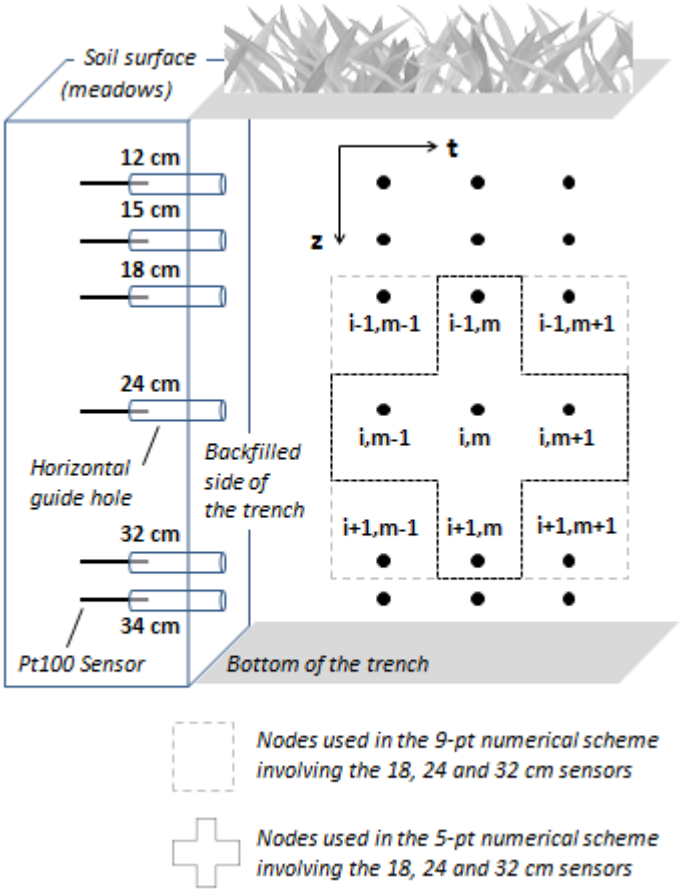

505

506

507 Fig. 1

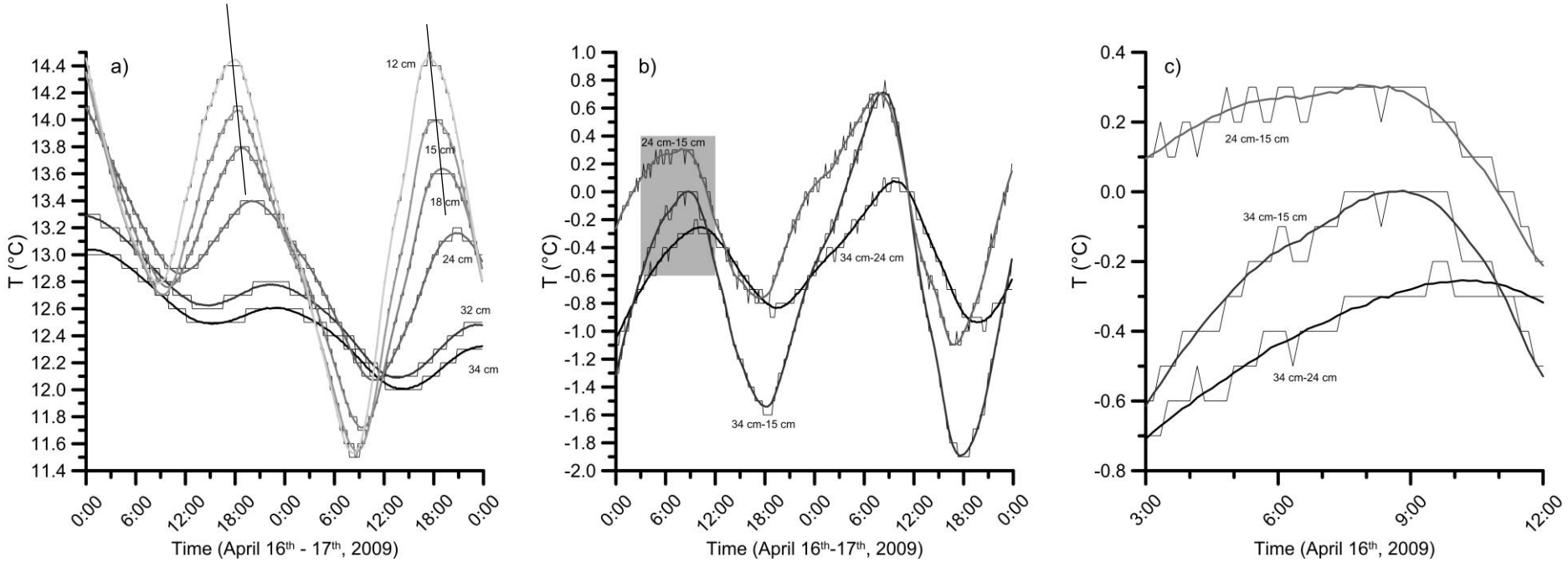

508

509 Fig. 2

510

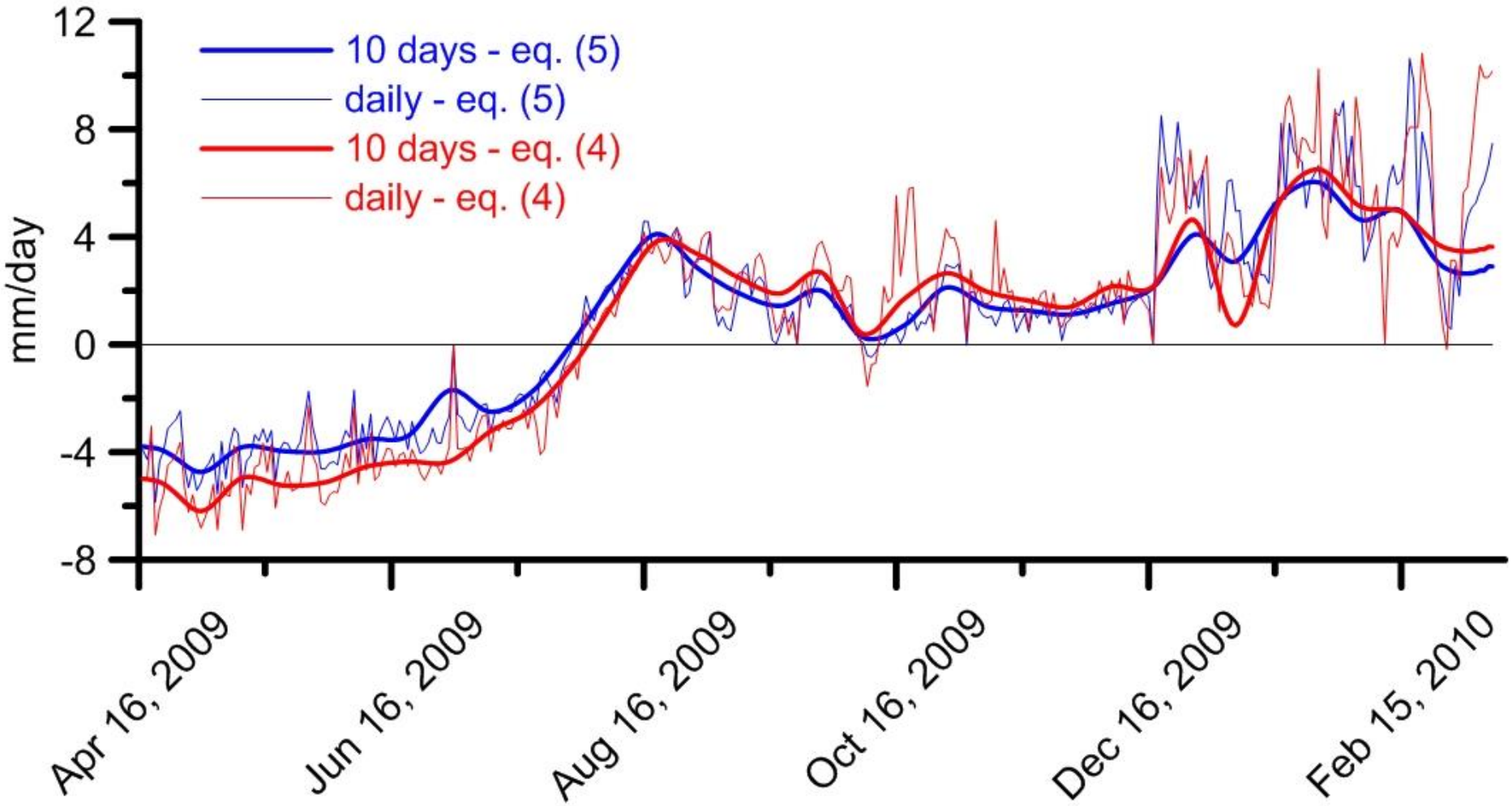
12
8
4
0
-4
-8
mm/day
10 days - eq. (5)
daily - eq. (5)
10 days - eq. (4)
daily - eq. (4)
Apr 16, 2009
Jun 16, 2009
Aug 16, 2009
Oct 16, 2009
Dec 16, 2009
Feb 15, 2010

Fig. 3

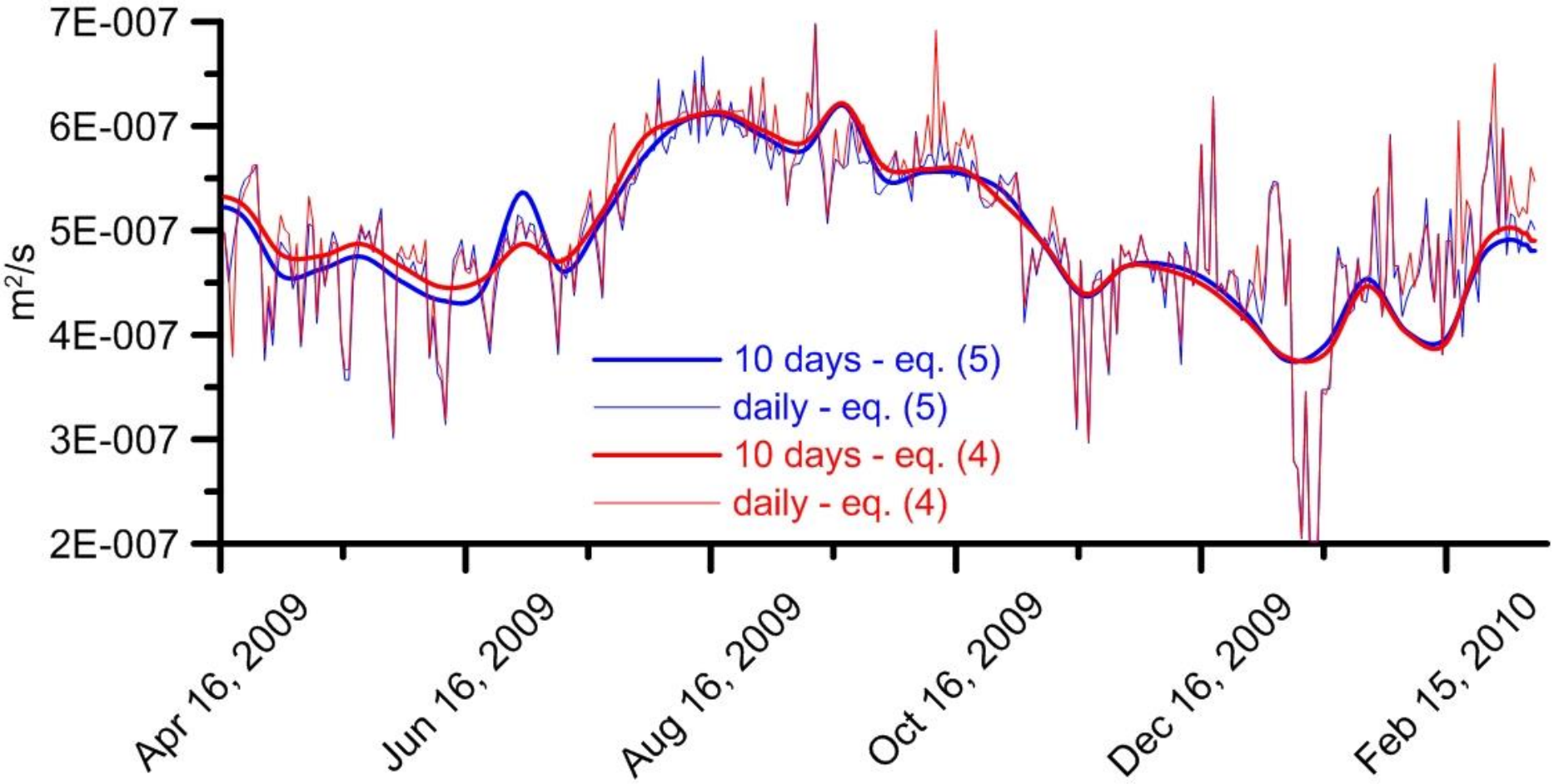
7E-007
6E-007
5E-007
4E-007
3E-007
2E-007
m²/s
10 days - eq. (5)
daily - eq. (5)
10 days - eq. (4)
daily - eq. (4)
Apr 16, 2009
Jun 16, 2009
Aug 16, 2009
Oct 16, 2009
Dec 16, 2009
Feb 15, 2010

Fig. 4

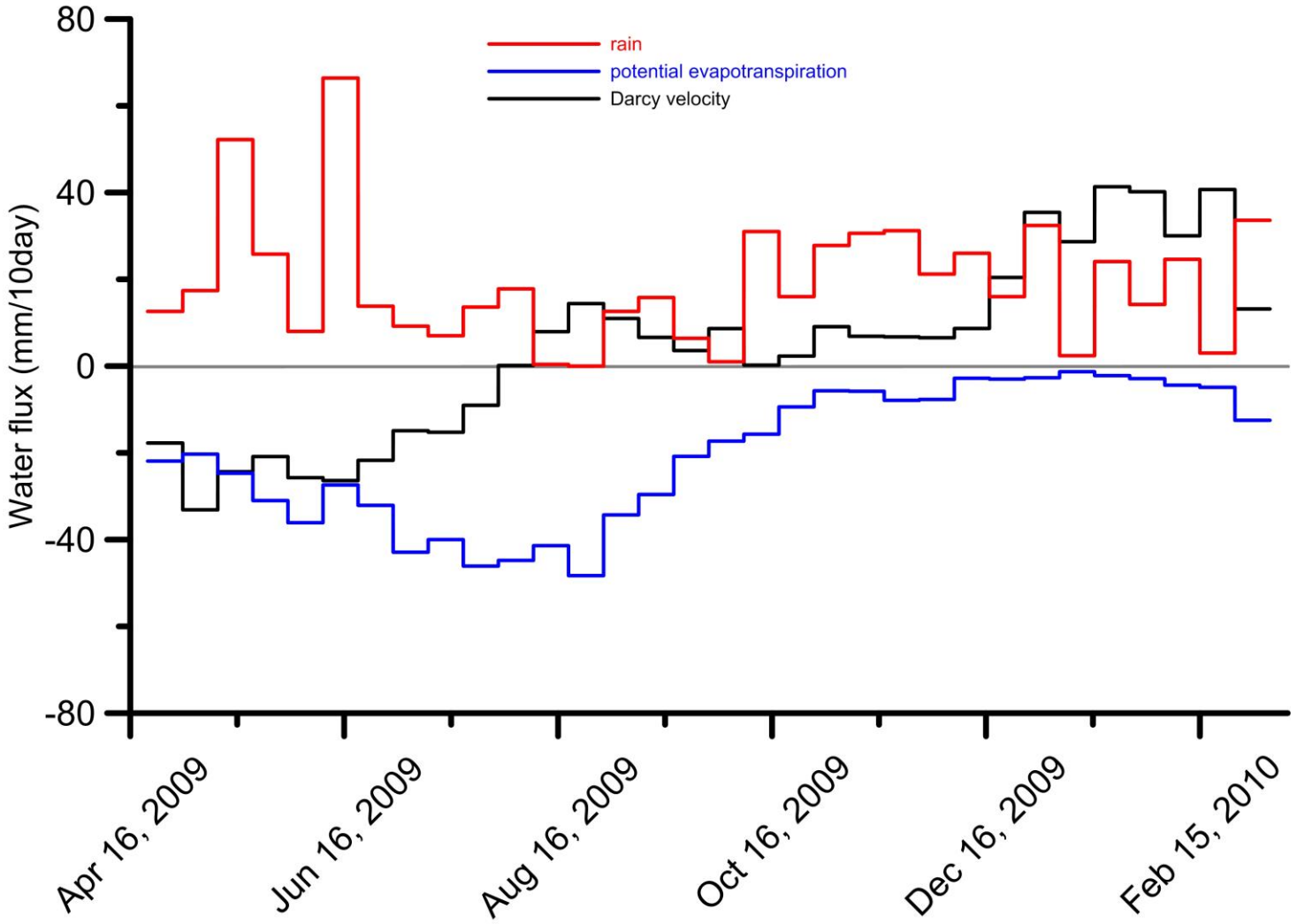

518

519 Fig. 5

520

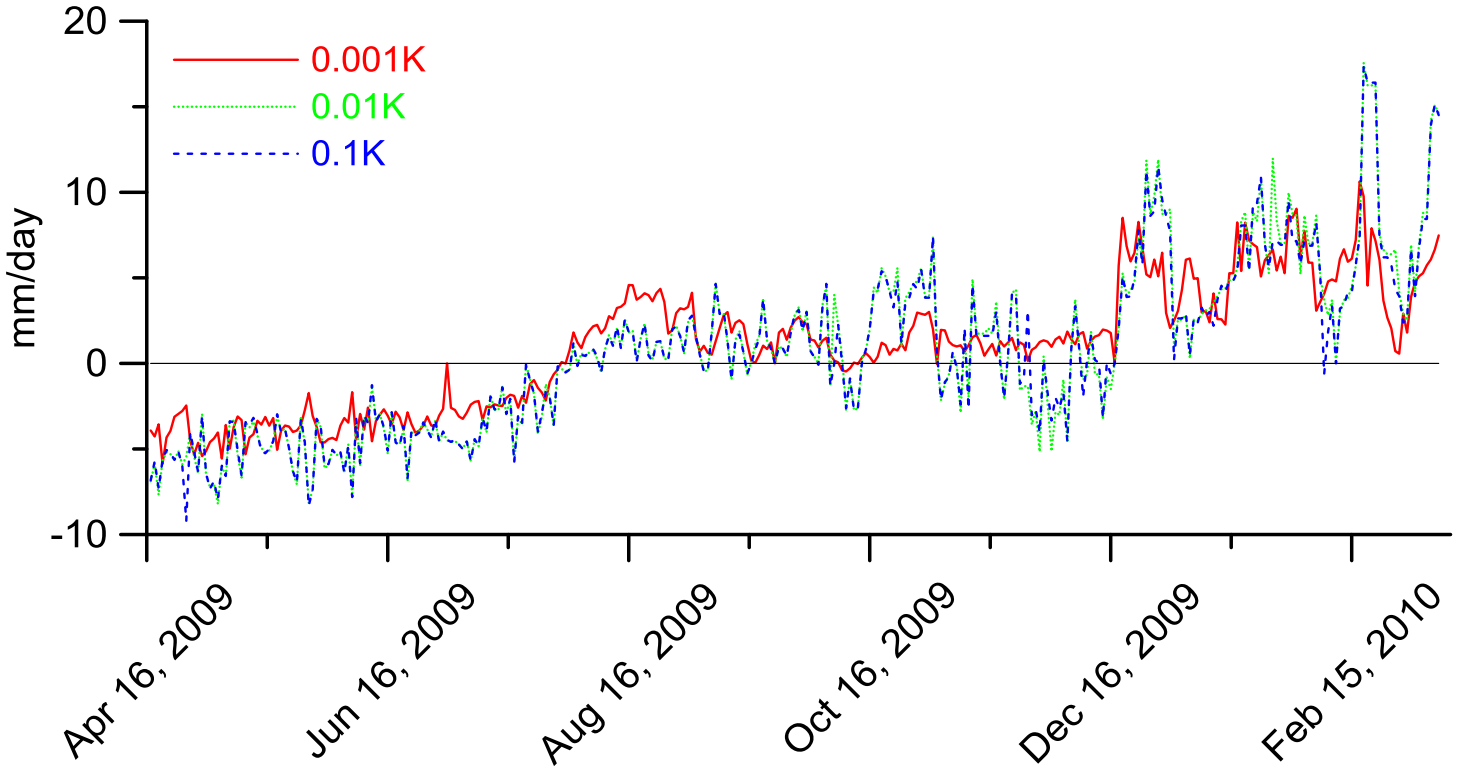
20
10
0
-10
mm/day
0.001K
0.01K
0.1K
Apr 16, 2009
Jun 16, 2009
Aug 16, 2009
Oct 16, 2009
Dec 16, 2009
Feb 15, 2010

Fig. 6a

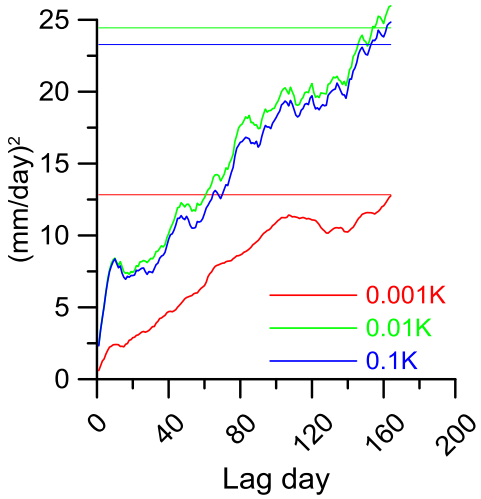
25
20
15
10
5
0
(mm/day)²
0.001K
0.01K
0.1K
0
40
80
120
160
200
Lag day

Fig. 6b

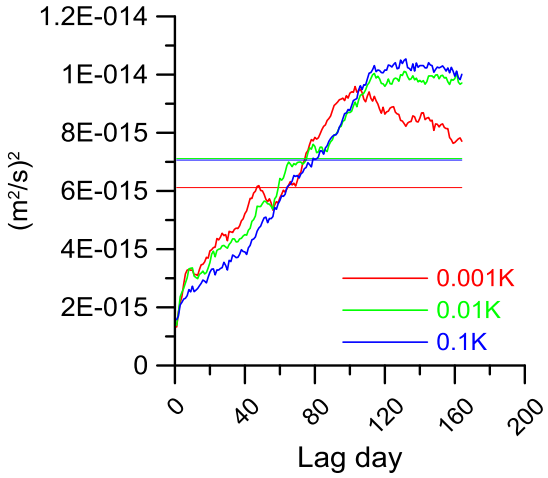
1.2E-014
1E-014
8E-015
6E-015
4E-015
2E-015
0
(m²/s)²
0.001K
0.01K
0.1K
0
40
80
120
160
200
Lag day

Fig. 6c

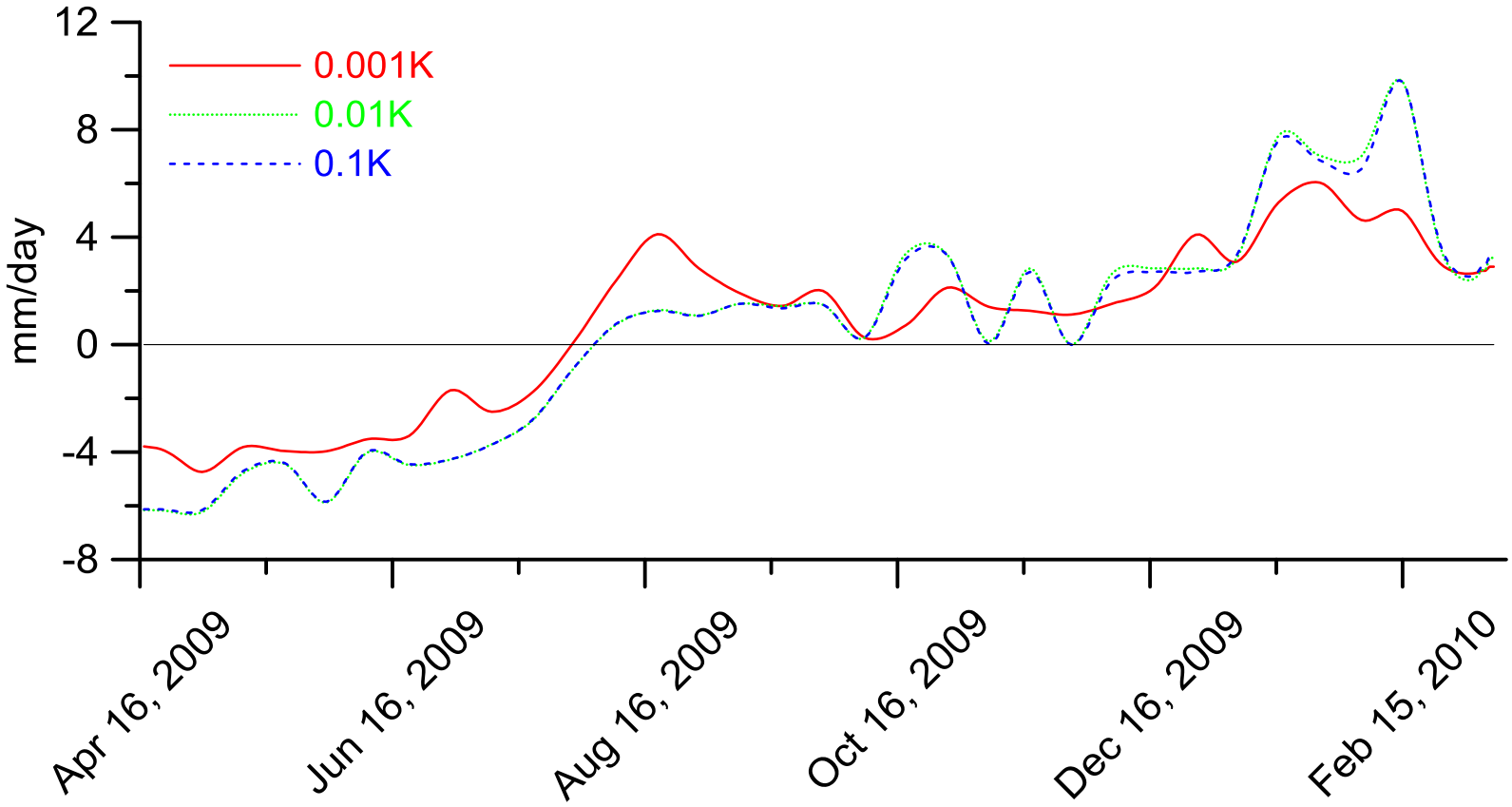

529

530 Fig. 7a

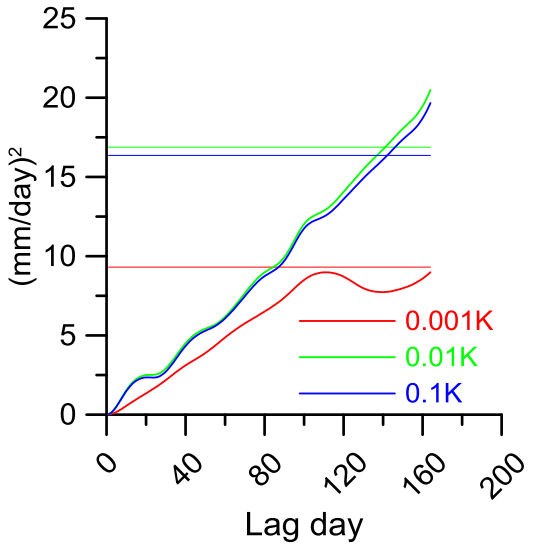
25
20
15
10
5
0
(mm/day)²
0.001K
0.01K
0.1K
0
40
80
120
160
200
Lag day

Fig. 7b

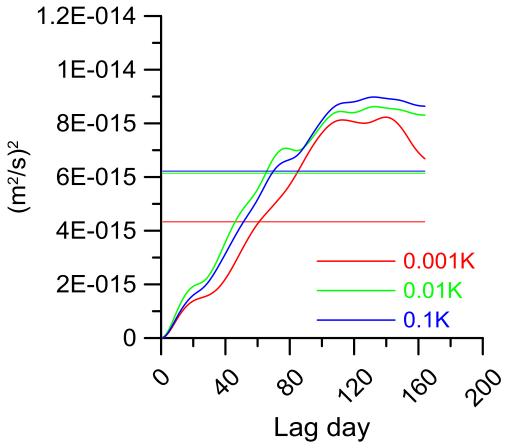
1.2E-014
1E-014
8E-015
6E-015
4E-015
2E-015
0
(m²/s)²
0.001K
0.01K
0.1K
0
40
80
120
160
200
Lag day

Fig. 7c

Depths of the three sensors (cm)	Mean quadratic deviations (mm d^{-1}) by reference to the calculations achieved with 15, 24 and 34 cm depths	
	Eq. (5)	Eq. (4)
14.9, 24, 34	0.160	0.164
15.1, 24, 34	0.163	0.250
15, 23.9, 34	0.289	0.350
15, 24.1, 34	0.265	0.230
15, 24, 33.9	0.112	0.083
15, 24, 34.1	0.146	0.150

Table 1

538

	Mean ($mm\ d^{-1}$)	Standard deviation ($mm\ d^{-1}$)	Median ($mm\ d^{-1}$)	Interquartile half distance ($mm\ d^{-1}$)
Eq. (4) 15, 24, 34 cm	1.23	3.98	1.36	3.30
Eq. (5) 15, 24, 34 cm	0.996	3.59	1.21	2.81

539 Table 2

540

Sensors at 15, 24, 34 cm	Global spectrum	First quarter from 0 to 0.125 d^{-1}	Second quarter from 0.125 to 0.25 d^{-1}	Third quarter from 0.25 to 0.375 d^{-1}	Fourth quarter from 0.375 to 0.5 d^{-1}
Eq. (4) Eq. (5)	0.954	0.960	0.109	0.048	0.142

541 Table 3

542

Eq. (5)	Global spectrum	First quarter from 0 to 0.125 d^{-1}	Second quarter from 0.125 to 0.25 d^{-1}	Third quarter from 0.25 to 0.375 d^{-1}	Fourth quarter from 0.375 to 0.5 d^{-1}
15, 24, 34 cm and 18, 24, 32 cm	0.976	0.980	0.506	0.188	0.406

543 Table 4